Journal of Power Sources 185 (2008) 501–511

Contents lists available at ScienceDirect

Journal of Power Sources

journal homepage: www.elsevier.com/locate/jpowsour

Chromium doping as a new approach to improve the cycling performance at high temperature of 5 V $LiNi_{0.5}Mn_{1.5}O_4$-based positive electrode

Mohamed Aklalouch[a,b], José Manuel Amarilla[a,*], Rosa M. Rojas[a], Ismael Saadoune[b], José María Rojo[a]

[a] Instituto de Ciencia de Materiales de Madrid, Consejo Superior de Investigaciones Científicas (CSIC) c/Sor Juana Inés de la Cruz, 3 28049 Madrid, Spain
[b] ECME, Faculté des Sciences et Techniques Marrakech, Université Cadi Ayyad, Av. A. El Khattabi, B.P.549 Marrakech, Morocco

ARTICLE INFO

Article history:
Received 28 March 2008
Received in revised form 8 May 2008
Accepted 28 June 2008
Available online 6 July 2008

Keywords:
Lithium battery
5 V electrode
Cathode
$LiMn_2O_4$
Spinel
$LiNi_{0.5}Mn_{1.5}O_4$

ABSTRACT

$LiCr_{2Y}Ni_{0.5-Y}Mn_{1.5-Y}O_4$ ($0 < Y \leq 0.2$) spinels have been synthesized by a sucrose-aided combustion method. Two sets of Cr-doped samples have been obtained by heating the "as-prepared" samples at 700 and 900 °C for 1 h. X-ray diffraction and thermogravimetric data show that pure and single phase spinels with similar lattice parameter have been synthesized. The homogeneity and the sub-micrometric particle size of the spinels have been shown by SEM and TEM. The main effect of the temperature is to increase the particle size from ≈50 to ≈500 nm, on heating from 700 to 900 °C. The study of the influence of Cr-dopant content and thermal treatment on the electrochemical properties at 25 °C and at 55 °C has been carried out by galvanostatic cycling in Li-cells. The discharge capacity (≈130 mAh g^{-1}) does not noticeably change with the synthesis conditions; but the cycling performances are strongly modified. Key factors that control the cycling performances have been determined. The most highlighted result is that spinels heated at 900 °C with $Y \leq 0.1$ have very high capacity retention at 55 °C (>96% after 40 cycles, cyclability >99.9% by cycle) indicating that metal doping is a new approach to prepare 5 V $LiNi_{0.5}Mn_{1.5}O_5$-based cathodes with excellent cycling performances at high temperature.

1. Introduction

$LiMn_2O_4$-based spinels are fairly attractive positive electrode (cathode) materials because they have remarkable advantages compared to the layered $LiCoO_2$ oxide widely used in commercial Li-ion batteries [1–4]. Among them, the most remarkable are: low cost, natural abundance of manganese ores, and environment friendliness. Mainly due to these advantages, $LiMn_2O_4$-based spinels are one of the best candidates as cathodes in large-size Li-ion batteries for applications as hybrid and electrical vehicles [5,6]. Nevertheless, the stoichiometric $LiMn_2O_4$ spinel shows large capacity fade during cycling [1,7,8], being it especially unacceptable at high temperature ($T \approx 55$ °C) [9,10]. The capacity fade mechanism of $LiMn_2O_4$-based cathodes is very complex because it depends on several factors, which usually operate at the same time. The most important are: (i) the structural transition due to Jahn–Teller distortion at the end of discharge [11,12], (ii) the slow dissolution of the spinel in the electrolyte [7,10,13,14], and (iii) the oxidation of the organic-based electrolyte on the electrode at the high potentials achieved at the end of charge [15–17].

It has been widely demonstrated that the cycling performances of $LiMn_2O_4$ can be notably improved by doping with metallic cations (M = Li^+, Ni^{2+}, Cr^{3+}, Co^{3+}, ...) which substituted the Mn^{3+} in the 16d octahedral sites of the spinel structure [7,18–21]. Moreover, Sigala et al. [18], showed for the first time that doping with Cr^{3+} leads to spinels in which a new electrochemical process at higher potential ($E \approx 4.9$ V) ascribed to Cr^{3+}/Cr^{4+} redox couple, was developed. Since then, many research groups have reinvestigated the $LiM_YMn_{2-Y}O_4$-doped spinels with the aim of developing new 5 V cathodes for Li-ion batteries [19,22–24]. The increase of cell voltage is very attractive because it allows raising the electric energy stored in the battery. Nowadays, these 5 V cathodes are being combined with anodes working at $E > 1$ V in order to assemble safer batteries [25,26].

Zhong et al. [19] first showed that $LiNi_{0.5}Mn_{1.5}O_4$ spinel was able to de-/inserted Li^+ in the 5 V region ($E \approx 4.7$ V). Since then, this material has been the most studied 5 V spinel-based cathode. In fact, development of $LiNi_{0.5}Mn_{1.5}O_4$-based cathodes is one of today's most important topics in Li-ion batteries [23,27–30]. Several studies have shown that the oxidation state of nickel in the $LiNi_{0.5}Mn_{1.5}O_4$ spinel is Ni^{2+} [29], and the Li^+ extraction/insertion take place in two steps assigned to Ni^{2+}/Ni^{3+} and Ni^{3+}/Ni^{4+} redox reactions [31]. The most remarkable advantage of $LiNi_{0.5}Mn_{1.5}O_4$ is its high cyclability. In fact, it is notably higher

* Corresponding author. Tel.: +34 913349074; fax: +34 913720623.
E-mail address: amarilla@icmm.csic.es (J.M. Amarilla).

0378-7753/$ – see front matter © 2008 Elsevier B.V. All rights reserved.
doi:10.1016/j.jpowsour.2008.06.074

than the one shown by other 5 V $LiM_YMn_{2-Y}O_4$ spinels [24]. The cyclability of $LiNi_{0.5}Mn_{1.5}O_4$ at room temperature can be even improved by doping [32–35] or optimizing the synthesis conditions [19,36,37]. Unfortunately, when cycling is carried out at 55 °C, the $LiNi_{0.5}Mn_{1.5}O_4$ shows a severe capacity fading that prevents its practical use [12,38]. Many efforts have been done to solve this drawback being the coating of $LiNi_{0.5}Mn_{1.5}O_4$ particles with some metal oxides the most explored way [12,39].

To the best of our knowledge, the effect of metal doping on the severe capacity fade of the $LiNi_{0.5}Mn_{1.5}O_4$ spinel at high temperature has not been studied yet. To perform this study, we have synthesized several Cr-doped spinels with general formula $LiCr_{2Y}Ni_{0.5-Y}Mn_{1.5-Y}O_4$ ($0 < Y \leq 0.2$). To maximize the 5 V capacity simultaneous substitution by Cr^{3+} for Ni^{2+} and Mn^{4+} has been done. The spinels have been synthesized by a sucrose-aided combustion method. This is a very useful method which offers good sample homogeneity, reduced the heat-treatment conditions, and allows synthesizing samples with small particle size [24]. Two sets of samples have been prepared by thermal treatment at 700 and 900 °C of the spinels obtained by the combustion method. The influence of Cr-content and heating temperature on the electrochemical properties at 25 °C and at 55 °C has been studied. Experiments focused to determine the factors that control the cycling performances have been also carried out. Finally, the electrochemical performances of our spinels are compared with selected doped and undoped-$LiNi_{0.5}Mn_{1.5}O_5$ spinels reported in the literature.

2. Experimental/materials and methods

$LiCr_{2Y}Ni_{0.5-Y}Mn_{1.5-Y}O_4$ ($Y = 0.05$, 0.1, 0.15 and 0.2) spinels have been synthesized by the sucrose-aided combustion method, from reagent grade Li(I), Cr(III), Ni(II) and Mn(II) nitrates, which act as the oxidants, and sucrose ($C_{12}H_{22}O_{11}$) as fuel. Stoichiometric amounts of Cr, Ni and Mn have been used; while a small excess of Li (5%) were used in order to compensate possible volatility during heating. After optimization of the combustion process, the mol number of sucrose chosen was 3/4. The reaction can be described as follows:

$$LiNO_3 + (2Y)Cr(NO_3)_3{\cdot}9H_2O + (0.5-Y)Ni(NO_3)_2{\cdot}4H_2O + (1.5-Y)Mn(NO_3)_2{\cdot}4H_2O + 3/4C_{12}H_{22}O_{11} \rightarrow LiCr_{2Y}Ni_{0.5-Y}Mn_{1.5-Y}O_4 + \text{gaseous byproducts}$$

Preset volumes of 1 M solutions of the corresponding metal M^{n+} nitrates ($M^{n+} = Li^+$, Cr^{3+}, Ni^{2+}, Mn^{2+}) were mixed. Sucrose was dissolved in the minimum amount of distilled water, and it was added to the nitrates solution. The solution was heated at ≈100 °C, and when dried it starts to swell up due to the evolution of gases generated in the thermolysis of the reagents, giving way to a foamy mass. Then, the temperature was increased at ≈140 °C. After a few minutes, the mass starts to burn up spontaneously without flame. The product of the reaction ("as-prepared" sample) is a very light and downy black powder. In order to prepare spinels with different particle size, the "as-prepared" samples were heated at 700 and 900 °C, 1 h in still air at 2 °C min^{-1} heating/cooling rate. Hereafter, the samples heated at 700 and 900 °C will be referred to SAC700 and SAC900, respectively.

The purity and particle size of the samples were studied by X-ray powder diffraction (XRD). X-ray patterns were recorded at room temperature in a Bruker D8 diffractometer, with Cu Kα radiation. The patterns were obtained in the step scanning mode at 0.04° (2θ) step and 2 s $step^{-1}$ counting time, within the range $15° \leq 2\theta \leq 80°$. Lattice parameters were refined with the CELREF program [40]. For SAC700 samples, the coherent crystallite domain has been calculated from several diffraction lines from the Scherrer formula: $D = (\lambda/\beta)\cos\theta$, where λ is the wavelength of Cu Kα = 1.54186 Å, θ is the diffraction angle, and $\beta = \sqrt{(\beta_m^2 - \beta_s^2)}$ is the corrected halfwidth of the diffraction peaks, where β_m is the observed halfwidth of the experimental diffraction peaks, and β_s is the halfwidth of the diffraction peaks of a standard sample, in our case the SAC900 sample with $Y = 0.2$.

Differential (DTA) and thermogravimetric (TG) analysis were carried out simultaneously with a DTA/TG Stamton STA 781 instrument up to 1000 °C in still air, and 10 °C min^{-1} heating/cooling rate. About 50 mg of sample was used in each run, and α-Al_2O_3 was the inert reference.

The morphology and the particle size of the samples were studied by scanning and transmission electron microscopy (SEM and TEM, respectively). SEM images were obtained in a JEOL JSM-5500 microscope. The samples, as powder, were covered with carbon by sputtering. TEM micrographs were taken in a JEOL 2000FX electron microscope operating at an acceleration voltage of 200 kV. The samples were dispersed in *n*-butyl alcohol, and drops of the dispersion were transferred to a holey carbon-coated copper grid.

The study of the dissolution of $LiCr_{2Y}Ni_{0.5-Y}Mn_{1.5-Y}O_4$ spinels in the 1 M $LiPF_6$ (EC/DMC) electrolyte was performed by soaking 80 mg of the samples in 10 ml of the electrolyte. The experiments were carried out in hermetic flasks into a dry box for 25 °C, and in hermetic flasks into a Buchi furnace for 55 °C. After 1 week, the solid and the electrolyte were separated by centrifugation at 6500 rpm for 15 min. The quantitative analysis of Cr, Ni and Mn cations dissolved in the electrolyte was performed by total-reflection X-ray fluorescence (TXRF). The TXRF spectra were recorded in a Slifert EXTRA-II spectrometer (Rich Seifert, Ahrensburg, Germany) equipped with a tungsten X-ray fine line and a Si(Li) detector with an active area of 80 mm^2 and a resolution of 157 eV at 5.9 keV (Mn, Kα). For the TXRF analysis, 2 μl of the solution was placed on a flat quartz carrier. The organic solvents were evaporated at 100 °C to obtain a solid homogeneous film.

The study of the electrochemical properties of the $LiCr_{2Y}Ni_{0.5-Y}Mn_{1.5-Y}O_4$ spinels was performed in a two-electrode lithium cell. Positive electrode composites containing ≈20 mg of spinel powder (72 wt.%), MMM Super P carbon black (17 wt.%), and poly(vinylidenefluorine-*co*-hexafluoropropylene) Kynar Flex® 2801 (PVdF-HFP, 11 wt.%) were made by suspending the powders in acetone as fugitive solvent. The percentages were chosen according to Reference [41]. Cylindrical pellets (12 mm diameter and ≈0.2 mm thickness) of positive electrode were obtained after cold pressing at 370 MPa. The negative electrode was a lithium foil, which also operated as reference electrode. The electrodes were separated by a Whatman BSF80 paper soaked in the electrolyte, which was a 1 M solution of $LiPF_6$ in ethylene carbonate and dimethyl carbonate (1:1, v/v) as supplied by UBE Europe GmbH. The components were assembled into a two-electrode Swagelock® cell within an argon glove box in which water content was kept below 1 ppm. The cell was galvanostatically cycled at 25 ± 0.5 °C in the voltage range of 3.4–5.2 V at 0.5*C*/1*C* charge/discharge rates with an Arbin battery tester system (BT2043). C is the capacity of the cathode in mAh calculated from the theoretical capacity of the $LiCr_{2Y}Ni_{0.5-Y}Mn_{1.5-Y}O_4$ spinel and the mass of spinel used in the composite. The coefficients of C rate are the inverse of the theoretical charge/discharge time expressed in hours. The electrochemical performances of the SAC900 samples at high-temperature were also determined. CR2032 coin cells were galvanostatically cycled at 0.5*C*/1*C* charge/discharge rate in the 3.4–5.2 V potential range at 55 ± 1 °C in a Buchi furnace. Measurements were carried out at least twice in order to guarantee the reproducibility of the electrochemical data. Electrochemical impedance of the cells was measured on IM6ex Electrochemical Workstation at room

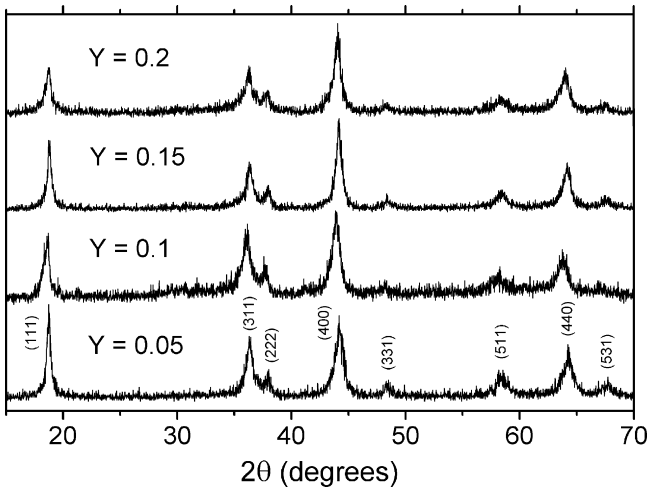

Fig. 1. X-ray diffraction patterns for the "as-prepared" $LiCr_{2Y}Ni_{0.5-Y}Mn_{1.5-Y}O_4$ ($0 < Y \leq 0.2$).

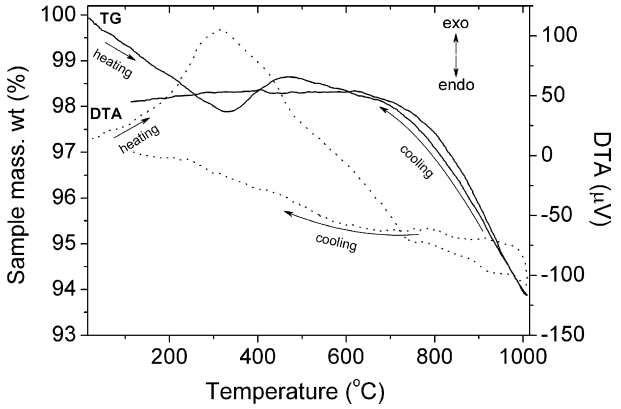

Fig. 2. TG (solid line) and DTA (dot line) heating/cooling curves recorded for the "as-prepared" $LiCr_{0.4}Ni_{0.3}Mn_{1.3}O_4$.

temperature. The amplitude of ac voltage was 5 mV, and the cells were measured at a constant potential after the appropriate equilibration. The frequency range was from 0.1 Hz to 100 kHz.

3. Results

3.1. Structural characterization

The X-ray patterns of the "as-prepared" $LiCr_{2Y}Ni_{0.5-Y}Mn_{1.5-Y}O_4$ samples are shown in Fig. 1. It is observed that all patterns are similar, showing broad diffraction peaks. They can be indexed according to a spinel-type structure in the *Fd*3*m* space group. Moreover, no significant displacements of the diffraction peaks on increasing the Cr-content ($2Y$) are observed; and hence, all the "as-prepared" samples have a similar cubic lattice parameter, $a_c \approx 8.18$ Å. The coherent crystalline domain determined from the Scherrer equation is small (≈9 nm) and similar for all the "as-prepared" samples.

The thermal analysis curves of the "as-prepared" samples are analogous. As an example, TG and DTA curves recorded simultaneously for the sample with $Y = 0.2$ are plotted in Fig. 2. A step and an exothermic peak are observed at ≈400 °C in the TG and DTA curves. Both effects, which have been also observed for other $LiNi_{0.5}Mn_{1.5}O_4$-based spinels synthesized by the combustion method [42], can be ascribed to the removal of some organic amorphous impurities not detected by XRD. So, it is necessary to heat the "as-prepared" samples at temperatures higher than 400 °C to eliminate the organic residues. At $T > 700$ °C, the decomposition of the spinel starts off, and a continuous weight loss take place up to at least 1000 °C. This weight loss is due to oxygen removal [36,43,44]. The TG curve recorded on cooling shows that the mass lost on heating is fully regained on cooling.

Two sets of spinels were synthesized heating the "as-prepared" samples at 700 and 900 °C. As an example, the X-ray patterns of the SAC700 and SAC900 spinels with $Y = 0.05$ and 0.2 are shown in Fig. 3. The patterns are alike, and there is not any noticeable displacement of the diffraction peaks either with the increase of the Cr-content or with the thermal treatment. Every pattern can be fully indexed in a cubic spinel cell, space group *Fd*3*m*. The nonappearance of the (2 2 0) peak at $2\theta \approx 30°$ indicates that there are no heavy atoms (Mn, Ni, Cr) in the 8a tetrahedral position. Moreover, it is not observe additional peaks due to crystalline impu-

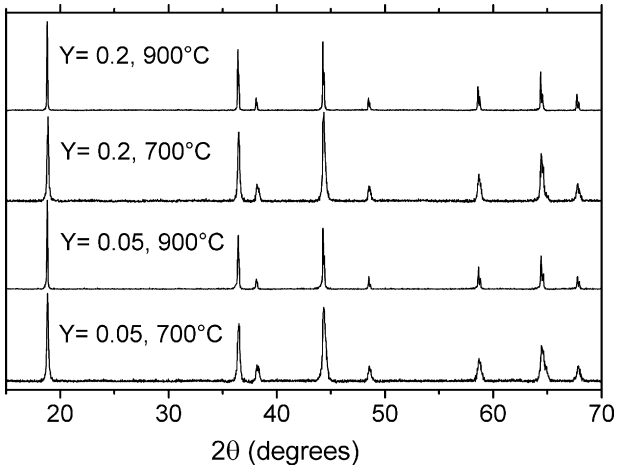

Fig. 3. X-ray diffraction patterns for the $LiCr_{2Y}Ni_{0.5-Y}Mn_{1.5-Y}O_4$ samples heated at 700 °C (SAC700) and 900 °C (SAC900) with $Y = 0.05$ and 0.2.

Table 1
Cubic lattice parameter and average particle size determined by X-ray diffraction, scanning and transmission electron microscopy for the $LiCr_{2Y}Ni_{0.5-Y}Mn_{1.5-Y}O_4$ spinels heated at 700 and 900 °C

Y in $LiCr_{2Y}Ni_{0.5-Y}Mn_{1.5-Y}O_4$	Thermal treatment	Lattice parameter (Å)	Average particle size by DRX or SEM (nm)	Average particle size by TEM (nm)
0.05	700 °C, 1 h	8.178(4)	28 (±15) [a]	33 (±9)
0.1	700 °C, 1 h	8.174(5)	31 (±10) [a]	–
0.15	700 °C, 1 h	8.173(6)	34 (±18) [a]	–
0.2	700 °C, 1 h	8.172(4)	34 (±17) [a]	47 (±12)
0.05	900 °C, 1 h	8.176(2)	520 (±220) [b]	578 (±160)
0.1	900 °C, 1 h	8.1754(5)	570 (±250) [b]	–
0.15	900 °C, 1 h	8.178(2)	500 (±275) [b]	–
0.2	900 °C, 1 h	8.1814(5)	470 (±350) [b]	480 (±147)

[a] Average particle size determined by DRX from the Scherrer equation.
[b] Average particle size determined by SEM.

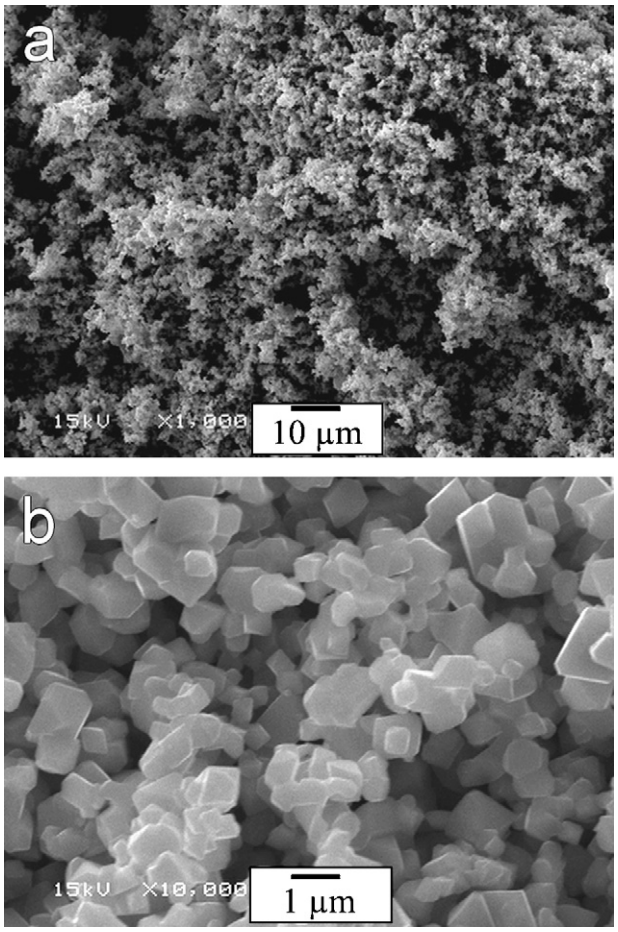

Fig. 4. SEM micrographs for the SAC900 samples: (a) $Y = 0.2$; (b) $Y = 0.1$.

rities. Similar results have been obtained for the others SAC700 and SAC900 samples. In consequence, we can conclude that cubic spinel $LiCr_{2Y}Ni_{0.5-Y}Mn_{1.5-Y}O_4$ single phases have been synthesized. This is a remarkable result because $LiNi_{0.5}Mn_{1.5}O_4$ samples synthesized by other procedures usually have NiO or Li_xNiO_2 as impurities [19,35,45]. The cubic lattice parameter, a_c, determined for the SAC700 and SAC900 samples are summarized in Table 1. As expected from the likeness on the peak position (Fig. 3), all SAC spinels have almost the same lattice parameter, $a_c \approx 8.175$ Å. Taking into account the ionic radius of $^{VI}Ni^{2+} = 0.69$ Å, $^{VI}Mn^{4+} = 0.53$ Å and $^{VI}Cr^{3+} = 0.615$ Å [46], the similarity of the lattice parameter can be explained by the random substitution of $1Ni^{2+} + 1Mn^{4+}$ by $2Cr^{3+}$ in the 16d octahedral positions. On the other hand, the fact that the lattice parameter does not increase with rising the heating temperature seems to indicate that oxygen vacancies, described for many $LiMn_2O_4$-based spinels heated at high temperatures [36,43,47], are not create for the SAC900 samples or their amount is very low. This is probably due to the very short thermal treatment time (1 h).

The main difference between the X-ray patterns of the SAC700 and SAC900 samples is the remarkable narrowing of the diffraction peaks on heating from 700 to 900 °C (Fig. 3). Narrowing could be explained by an increase of the particle size with raising the heated temperature. The coherent crystallite domain determined by the Scherrer formula for the SAC700 spinels is ≈50 nm (Table 1). For the SAC900 spinels, the strong shrinkage of the diffraction maxima does not allow determining the particle size from X-ray data.

3.2. Textural and morphological characterization

The morphology and the particle size of the SAC900 spinels have been investigated by scanning electron microscopy. As an example, SEM micrographs of samples with $Y = 0.1$ and 0.2 at different magnifications are shown in Fig. 4. The image at lower magnification (Fig. 4a) illustrates the high homogeneity of the spinels synthesized. At higher magnification (Fig. 4b), it is observed that the particles are homogeneous, exhibit surface facets and they are not too much sintered. The particle size determined by SEM is outlined in Table 1. The SAC900 spinels have a similar particle size of ≈500 nm; that is, all they are sub-micrometric.

The evolution of particle size with heated temperature has been studied by transmission electron microscopy. Fig. 5 shows the TEM micrographs of the spinels with $Y = 0.05$ and 0.2 heated at 700 and 900 °C. The particle size histograms for the two samples with $Y = 0.05$, and the best fittings to Gaussian curves are also drawn. The average particle sizes and the corresponding standard deviation are summarized in Table 1. The analysis of the data shows that the main effect of the heated temperature rise is the remarkable increase of the particle size. In fact, it increases from 33 nm for the SAC700 with $Y = 0.05$ to 578 nm for the corresponding SAC900 one. Nevertheless, it is important to remark that all $LiCr_{2Y}Ni_{0.5-Y}Mn_{1.5-Y}O_4$ spinels synthesized by the sucrose-aided combustion method have a small particle size, being it <1 μm. This is an interesting issue because electrode materials with sub-micron particle size notably improve their electrochemical properties; for instance, its rate capability. The small particle size of the samples could be explained assuming that gases evolved during the combustion cause a spreading out of the reaction mass separating the particles as shows the spongy morphology of the samples (Fig. 4). In addition, the spreading out can also help to dissipate the heat generated during the burning and hence, inhibiting the sintering of the particles.

3.3. Electrochemical properties

3.3.1. Electrochemical properties at room temperature

The electrochemical properties of $LiCr_{2Y}Ni_{0.5-Y}Mn_{1.5-Y}O_4$ spinels at 25 °C have been determined by galvanostatic studies at high current (1*C* discharge rate) in the potential range 3.4–5.2 V. Fig. 6 shows the 2nd charge/discharge curves of the SAC700 and SAC900 samples with $Y = 0.05$ and 0.2. Similar curves have been obtained for the others spinels synthesized. The 2nd discharge capacities (Q_d) determined from the galvanostatic curves are summarized in Table 2. It is observed that Q_d values are high and very close (≈125 mAh g^{-1}); that is, the discharge capacity does not noticeably change either with the Cr-content or with the heated temperature. These results are better than those shown by $LiCo_{2Y}Ni_{0.5-Y}Mn_{1.5-Y}O_5$ spinels for which the capacity decreases with increasing the Co-dopant content [42]. The likeness observed for the capacities can be explained assuming the next electrochemical reaction (Eq. (1)).

$$LiCr_{2Y}{}^{3+}Ni_{0.5-Y}{}^{2+}Mn_{1.5-Y}{}^{4+}O_4 \leftrightarrow Cr_{2Y}{}^{4+}Ni_{0.5-Y}{}^{4+}Mn_{1.5-Y}{}^{4+}O_4 + (Li^+ + e^-) \quad (1)$$

As the molecular weight of the $LiCr_{2Y}Ni_{0.5-Y}Mn_{1.5-Y}O_4$ ($0 < Y \leq 0.2$) spinels is similar and, regardless the Cr-dopant content, one Li^+/e^- can be de-/inserted (Eq. (1)); the theoretical capacity (Q_t) for all the spinels must be very close. In fact, Q_t only increases from 147.1 to 148.3 mAh g^{-1} for samples from $Y = 0.05$ to 0.2. Moreover, as the crystalline structure and composition of the spinels does not change on increasing the heated temperature (Fig. 3, Table 1), the capacity of the SAC700 and SAC900 spinels must be also similar,

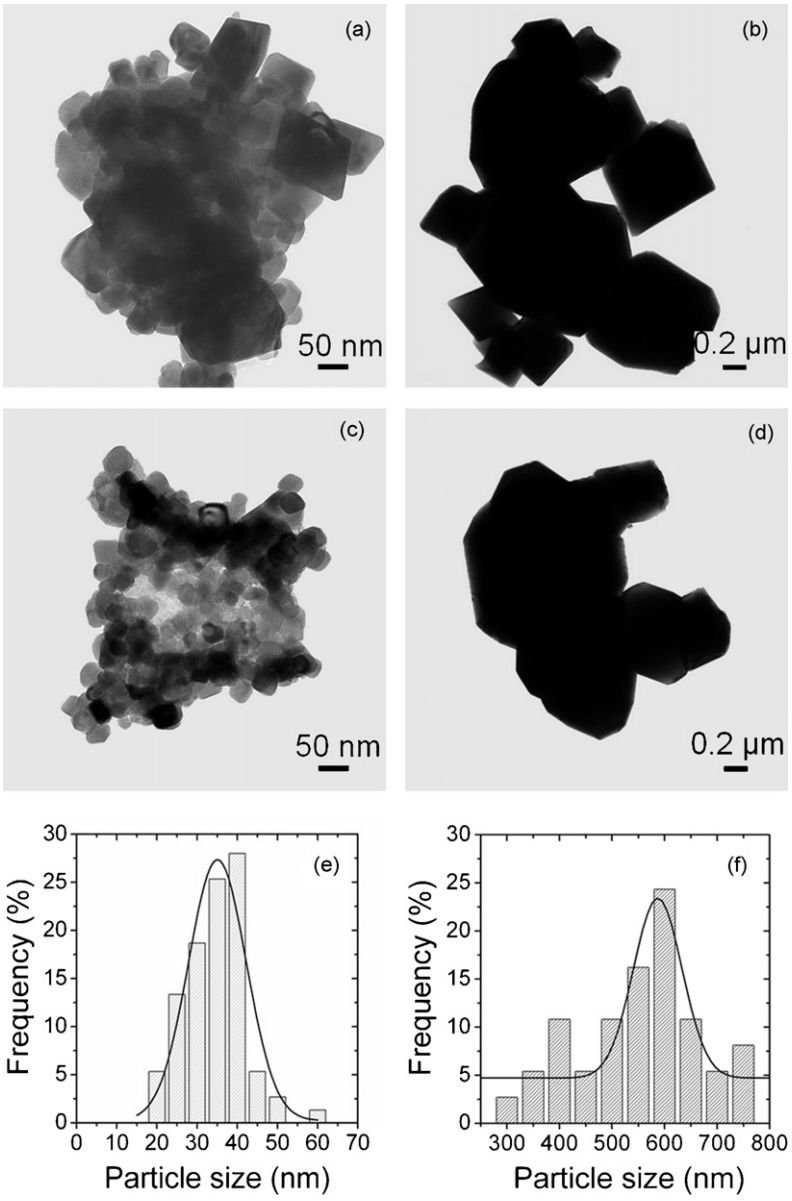

Fig. 5. TEM micrographs for $LiCr_{0.4}Ni_{0.3}Mn_{1.3}O_4$ heated at: (a) 700 °C; (b) 900 °C; and for $LiCr_{0.1}Ni_{0.45}Mn_{1.45}O_4$ heated at: (c) 700 °C; (d) 900 °C. Histograms: (e) of the sample shown in c, (f) of the sample shown in (d).

as has been experimentally observed (Table 2). From Eq. (1), we can establish that Cr^{3+} and Ni^{2+} are the cations electrochemically actives in the 5 V region. This assertion well agrees with results previously reported [19,29,48,49]. It is worth to remark that even at the high current used (1*C* discharge rate), the capacity of the samples is close to the corresponding theoretical one. This result shows that all the spinels synthesized by the SAC method exhibit a high rate capability. This property can be explained by the sub-micron particle size and the porous texture of the samples synthesized (Fig. 4, Table 1).

The analysis of the shape of the charge/discharge curves (Fig. 6) shows that they have a large plateau at ≈4.7 V (hereafter named 5 V region, $Q_{5V} > 100\ mAh\ g^{-1}$) and a very small plateau at ≈4 V ($Q_{4V} < 10\ mAh\ g^{-1}$). According to Eq. (1), the large plateau in the 5 V region must be ascribed to $Cr^{3+}$and Ni^{2+} redox reactions. The small plateau at ≈4 V, which is observed in most of the $LiNi_{0.5}Mn_{1.5}O_4$-based cathodes [29,33,35,42], is due to the presence of residual amount of Mn^{3+} in the spinel. A deeply analysis of the curves shows that the large plateau in the 5 V region become more sloping on increasing the Cr content. To understand this result, we have studied several spinels by slow cycling voltammetry ($0.1\ mV\ s^{-1}$). In Fig. 7, the voltammograms of the SAC900 samples with $Y = 0.05$ and 0.1 are compared. In the 5 V region, both samples show three well-defined peaks at ca. 4.6, 4.7 and 4.8 V in discharge. The intensity of the peaks at 4.6 and 4.7 V decreases on increasing the Cr-content. As Ni^{2+} and Cr^{3+} are the cations actives in the 5 V region (Eq. (1)), it is reasonably to assign these two peaks to Ni^{2+} redox reactions. It has been shown that oxidation of Ni^{2+} in $LiNi_{0.5}Mn_{1.5}O_4$ takes place in two well-defined steps due to Ni^{2+}/Ni^{3+} and Ni^{3+}/Ni^{4+} redox couples [31]. The third peak centred at 4.8 V, for which the intensity increases on increasing the Cr-content, is assigned to Cr^{3+}/Cr^{4+} redox couple. From the cycling voltammetry data, the increase of the slope of the 5 V plateau with the Cr-content can be explain by: (i) the decrease of the intensities of the two Ni^{2+}-peaks, (ii) the simultaneous increase of the Cr^{3+}-peak at higher potential, and (iii) the overlapping of the three peaks. A similar behavior was observed

Table 2
The 2nd discharge capacity, lithium insertion degree, capacity retention after 40 cycles (QRt-40), cyclability (cc), and average coulombic efficiency (C_{Eff}) determined for the $LiCr_{2Y}Ni_{0.5-Y}Mn_{1.5-Y}O_4$ spinels heated at 700 and 900 °C

Y in $LiCr_{2Y}Ni_{0.5-Y}Mn_{1.5-Y}O_4$	Thermal treatment	Cycling temperature (°C)	2nd discharge capacity (mAh g^{-1})	Li^+ insertion degree	QRt-40 (%)	Cyclability (% by cycle)	C_{Eff} (%)
0.05	700 °C, 1 h	25	128	0.87	80.94	99.51	97.92
0.1	700 °C, 1 h	25	123	0.83	81.12	99.50	97.41
0.15	700 °C, 1 h	25	122	0.82	74.47	99.32	96.6
0.2	700 °C, 1 h	25	123	0.83	65.93	98.95	95.55
0.05	900 °C, 1 h	25	127	0.86	99.20	99.99	98.88
0.1	900 °C, 1 h	25	128	0.87	98.89	99.99	99.09
0.15	900 °C, 1 h	25	123	0.83	97.40	99.98	98.78
0.2	900 °C, 1 h	25	132	0.89	93.06	99.80	98.78
0.05	900 °C, 1 h	55	132	0.90	96.52	99.93	98.84
0.1	900 °C, 1 h	55	140	0.95	97.03	99.93	98.65
0.15	900 °C, 1 h	55	129	0.87	92.07	99.76	97.7
0.2	900 °C, 1 h	55	131	0.88	80.5	99.54	97.84

for $LiCo_{2Y}Ni_{0.5-Y}Mn_{1.5-Y}O_4$ spinels with increasing the Co-dopant [42].

The study of the cycling performances of the SAC700 and SAC900 spinels at 25 °C has been carried out by cycling test cells at 0.5C/1C charge/discharge rates in the 3.4–5.2 V voltage region. As an example, Fig. 8 shows a selection of charge/discharge curves recorded during cycling of the $LiCr_{0.3}Ni_{0.35}Mn_{1.35}O_4$ (Y = 0.15) heated at 700 and 900 °C. It is clearly observed that the cycling behavior of both spinels is different. For the SAC700 sample (Fig. 8a), the discharge capacity notably decreases from 122 to 92 mAh g^{-1} after 40 cycles; i.e., it shows a poor cycling performance. In an opposite way, the reversibility exhibited by the SAC900 sample is very high (Fig. 8b). In fact, the capacity only diminishes from 123 to 122 mAh g^{-1} (2nd and 40th cycles, respectively). For the same cycle, when the charge and discharge capacities (Q_c, Q_d) are compared, it is observed that both are similar for the SAC900 sample; nevertheless, Q_c is remarkably higher than Q_d for the SAC700 spinels. These results are more clearly observed in Fig. 8c in which variation of Q_c and Q_d vs. cycle number has been plotted. Similar results have been obtained for the other Cr-doped spinels synthesized. That indicate the coulombic efficiency notably decreases with increasing the heating temperature.

The evolution of the discharge capacity vs. cycle number for the SAC700 and SAC900 spinels registered at 25 °C is compared in Fig. 9. The analysis of the plots permits us to assert that the cycling behavior of $LiCr_{2Y}Ni_{0.5-Y}Mn_{1.5-Y}O_4$ spinels strongly depends on the synthesis conditions. From the cycling data we have determined the capacity retention after 40 cycles (QRt-40) and the cyclability (cc). This latter has been calculated from the equation $Q_n = Q_1 cc^{(n-1)}$ where Q_1 and Q_n are the discharge capacities for the 1st and nth cycles, respectively. The values in percentage for QRt-40 and cc are summarized in Table 2. The SAC700 samples with $Y \leq 0.1$ show moderate retention capacities (QRt-40 ≈ 81% after 40 cycles) and they notably decrease with increasing the Cr-content (QRt-40 = 65.93% for Y = 0.2). For the SAC900 spinels, QRt-40 is >90% in all cases. Besides, the cyclability of the samples with $Y \leq 0.1$ is very high (cc = 99.99%). From this cyclability, the cycle life (cycle number for which $Q_n = 0.8Q_1$) of the former SAC900 spinels is >2000 cycles. These results show that SAC900 spinels with $Y \leq 0.1$ exhibit excellent cycling performances at 25 °C. In all cases, they are better than those for SAC700.

3.3.2. Electrochemical performances at 55 °C

It was previously indicated that the main drawback of the $LiNi_{0.5}Mn_{1.5}O_4$ spinel is the severe capacity loss when cycling is carried out at high temperature (50–60 °C) [12,38,45]. In this way, we have considered essential to study the electrochemical properties of the SAC900 spinels at high temperature. These samples have been chosen because they showed the best cycling performances at room temperature. Fig. 10 compares the 2nd charge/discharge curves for the SAC900 spinels registered at 55 °C. All curves are similar, showing the characteristic plateau in the

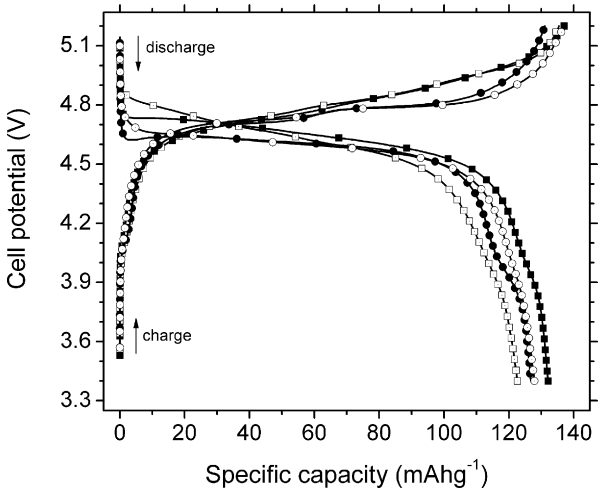

Fig. 6. The 2nd charge/discharge curves registered at 25 °C for the samples with Y = 0.05 and 0.2 heated at 700 °C (open circle and square, respectively), and at 900 °C (closed circle and square, respectively). Charge/discharge were carried out at 0.5C/1C rates.

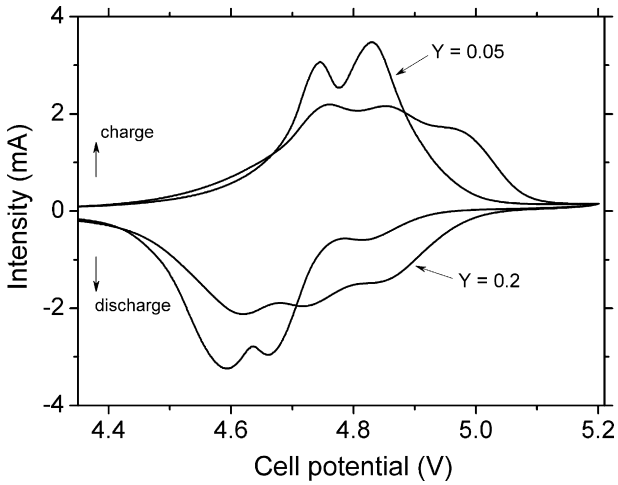

Fig. 7. Cyclic voltammograms for the SAC900 spinels with Y = 0.05 and 0.2. Potential sweep speed was 0.1 mV s^{-1} at 25 °C.

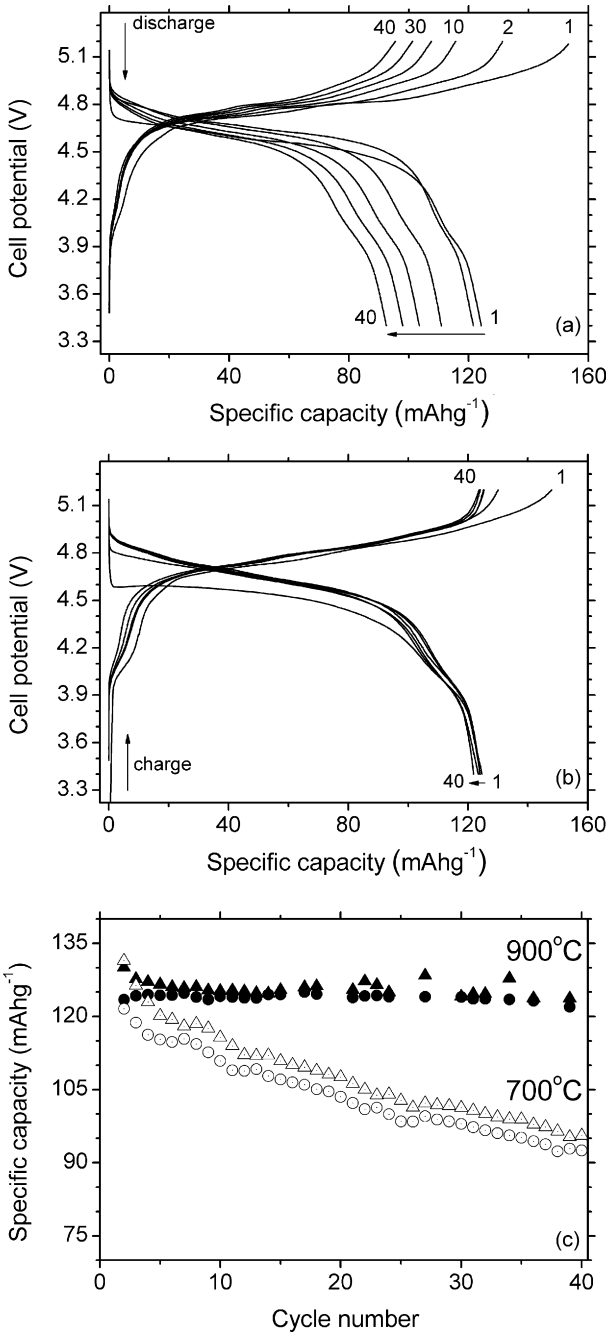

Fig. 8. Selected charge/discharge curves obtained during cycling at 25 °C for the $LiCr_{0.3}Ni_{0.35}Mn_{1.35}O_4$ spinel heated at: (a) 700 °C; (b) 900 °C. (c) Evolution of charge (triangle) and discharge (square) capacity vs. cycle number for both samples. Charge/discharge were carried out at 0.5*C*/1*C* rates.

4.7 V voltage region ascribed to Cr^{3+} and Ni^{2+} redox reactions (Eq. (1)). Curves are also analogous to those obtained at 25 °C (Fig. 6). The capacity of the SAC900 spinels and the corresponding Li^+-insertion degree (ΔLi^+) determined from the 2nd discharge are summarized in Table 2. The SAC900 spinels have a high capacity ($Q_d \approx 130\,mAh\,g^{-1}$) being the insertion degree >0.85 Li^+. Discharge capacity does not change with the Cr-content; nevertheless, it is slightly higher than those at 25 °C (Table 2). As the discharge rate was elevated (1*C*), the increase of Q_d observed could be explained by the raise of the Li^+ insertion kinetics when increasing the cycling temperature.

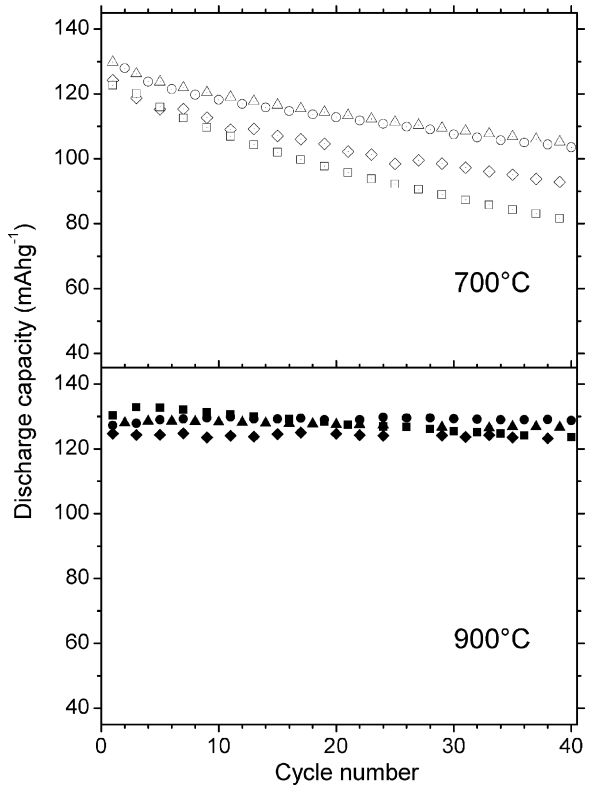

Fig. 9. Evolution of the discharge capacity at 25 °C vs. cycle number for SAC700 and SAC900 $LiCr_{2Y}Ni_{0.5-Y}Mn_{1.5-Y}O_4$ spinels (circle, $Y = 0.05$; triangle, $Y = 0.1$; rhomb, $Y = 0.15$; square, $Y = 0.2$). Charge/discharge were carried out at 0.5*C*/1*C* rates.

The cycling performances at 55 °C have been also studied. In Fig. 11 the variation of discharge capacity vs. cycle number is plotted. The capacity retention after 40 cycles and the cyclability are summarized in Table 2. The most remarkable result is the excellent cycling performances of the SAC900 samples with $Y \leq 0.1$ which have cyclabilities >99.9%. This result permits us to show that doping allows preparing 5 V $LiNi_{0.5}Mn_{1.5}O_4$-based cathodes with excellent cycling performances at high temperature. For the SAC900 spinels with $Y > 0.1$, the cycling performances worsen with increasing the

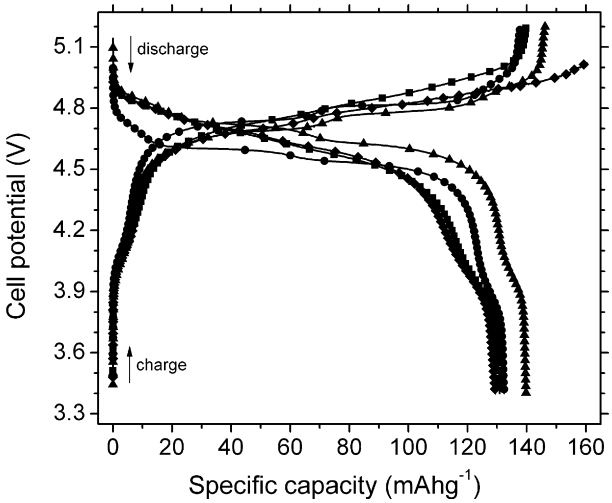

Fig. 10. The 2nd charge/discharge curves registered at 55 °C for SAC900 $LiCr_{2Y}Ni_{0.5-Y}Mn_{1.5-Y}O_4$ spinels (circle, $Y = 0.05$; triangle, $Y = 0.1$; rhomb, $Y = 0.15$; square, $Y = 0.2$). Charge/discharge were carried out at 0.5*C*/1*C* rates at 55 °C.

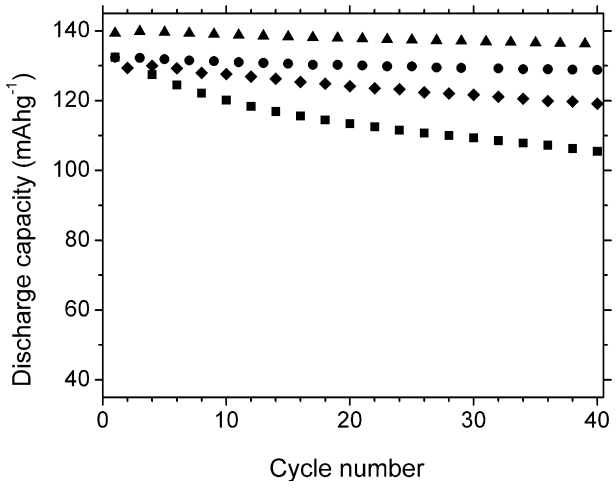

Fig. 11. Evolution of the discharge capacity at 55 °C vs. cycle number for the SAC900 $LiCr_{2Y}Ni_{0.5-Y}Mn_{1.5-Y}O_4$ spinels (circle, $Y = 0.05$; triangle, $Y = 0.1$; rhomb, $Y = 0.15$; square, $Y = 0.2$). Charge/discharge were carried out at 0.5*C*/1*C* rates.

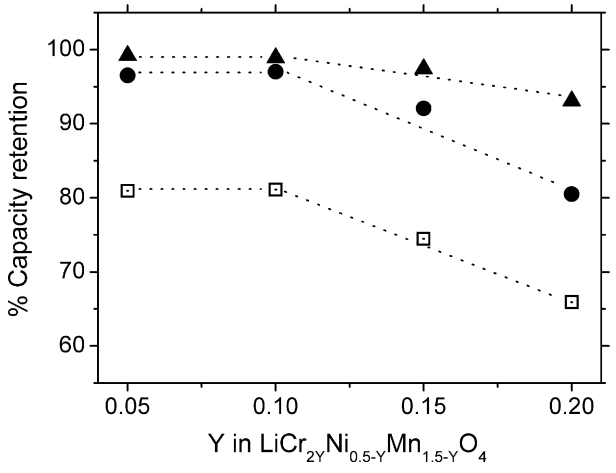

Fig. 12. Capacity retention after 40 cycles vs. Y in $LiCr_{2Y}Ni_{0.5-Y}Mn_{1.5-Y}O_4$ for SAC700 samples at 25 °C (square), and for SAC900 samples at 25 °C (triangle) and at 55 °C (circle).

Cr-content, being QRt-40 significantly lower than those determined at 25 °C. We have also determined the coulombic efficiency in percent (C_{Eff}) as the average value of ($Q_{nd} \times 100/Q_{nc}$) for the cycles from $n = 10$ to 40. The C_{Eff} values for the SAC700 and SAC900 spinel at 25 and 55 °C cycling temperatures are summarized in Table 2. The analysis of the data shows that the coulombic efficiency remarkably depends on the synthesis conditions. It increases with decreasing the Cr-content and/or with raising the heated temperature.

4. Discussion

We were very interested to study the factors that control the cycling performances of the $LiCr_{2Y}Ni_{0.5-Y}Mn_{1.5-Y}O_4$ spinels. To achieve this objective we first analyzed the evolution of the capacity retention (QRt-40) vs. Y in $LiCr_{2Y}Ni_{0.5-Y}Mn_{1.5-Y}O_4$ for the SAC700 at 25 °C and for the SAC900 at 25 and 55 °C. The results in Fig. 12 clearly reveal that the cycling performances depend on the Cr-content, thermal treatment and cycling temperature. On increasing the Cr content, two well-defined regions are observed: (i) for samples with $Y \leq 0.1$, QRt-40 remains constant (≈81 and ≈98% for SAC700 and SAC900 samples, respectively), and (ii) for samples with $Y > 0.1$, QRt-40 decreases on increasing the Cr content. Refer to the thermal

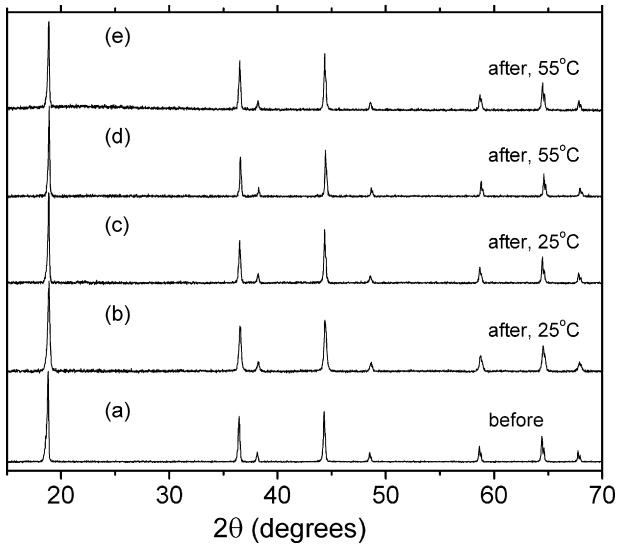

Fig. 13. X-ray diffraction patterns for pellets of the composite cathodes: (a) SAC900 with $Y = 0.1$ before cycling, (b) SAC700 with $Y = 0.1$, and (c) SAC900 with $Y = 0.1$ after cycling at 25 °C; (d) SAC900 with $Y = 0.05$, and (e) SAC900 with $Y = 0.2$ after cycling at 55 °C.

treatment; the capacity retention of the SAC900 spinels is always higher than those of SAC700, even when SAC900 were cycled at 55 °C. Nevertheless, the most important results to remark is that QRt-40 at 25 and 55 °C are very close (≈99 and ≈97%, respectively) for the SAC900 spinels with $Y \leq 0.1$. This result shows again that doping of the $LiNi_{0.5}Mn_{1.5}O_4$ with small amounts of Cr^{3+} ($2Y \leq 0.2$) allow synthesizing 5 V cathode materials with high cyclability at 55 °C. Thus, we can conclude that doping with chromium cations is a right way to overcome the severe capacity loss usually described for $LiNi_{0.5}Mn_{1.5}O_4$-based cathodes when they are cycled at high temperature.

It was previously indicated in the introduction that key factors responsible for the capacity fade of $LiMn_2O_4$-based cathodes are: (i) structural transformations happening during cycling [11,12], (ii) dissolution of the spinel into the electrolyte [7,10,13,14], and (iii) oxidation of the electrolyte on charging [15–17]. We have analyzed these factors to realize if they can account for the variation of cycling performances observed for our $LiCr_{2Y}Ni_{0.5-Y}Mn_{1.5-Y}O_4$ spinels (Fig. 12). To test if some structural modifications happened, we recorded the XRD patterns of cathodes after cycling. Pellets were dried but they were not washed to avoid removal of possible precipitated phases on the pellet surface. As an example, in Fig. 13 the X-ray patterns of several cathodes after cycling at 25 °C or at 55 °C are compared with this of the pristine $LiCr_{0.2}Ni_{0.4}Mn_{1.4}O_4$ heated at 900 °C. The patterns of cathodes after cycling are practically identical among them and to the pristine $Y = 0.1$ spinel. In fact, no noticeable changes either in the peak positions or in the peak intensities are observed. Moreover, the nonappearance of the (2 2 0) diffraction peak of the spinel at $2\theta \approx 30°$ shows that there are not displacements of heavy cations to the 8a tetrahedral positions during cycling as it was described for Cr-doped $LiMn_2O_4$ [50]. Extra peaks due to crystalline impurities have neither been observed. All these results show that $LiCr_{2Y}Ni_{0.5-Y}Mn_{1.5-Y}O_4$ spinels have not undergone any noticeable structural modification during cycling. In consequence, this factor is not at the origin of the variation of capacity retention observed.

Other source of the failure mechanism of $LiMn_2O_4$-based cathodes is the dissolution of the spinel in the electrolyte [7,10,14,49]. Some moisture in $LiPF_6$ organic-based electrolytes reacts with PF_6^- anions giving way to HF, which is the acid responsible of the spinel

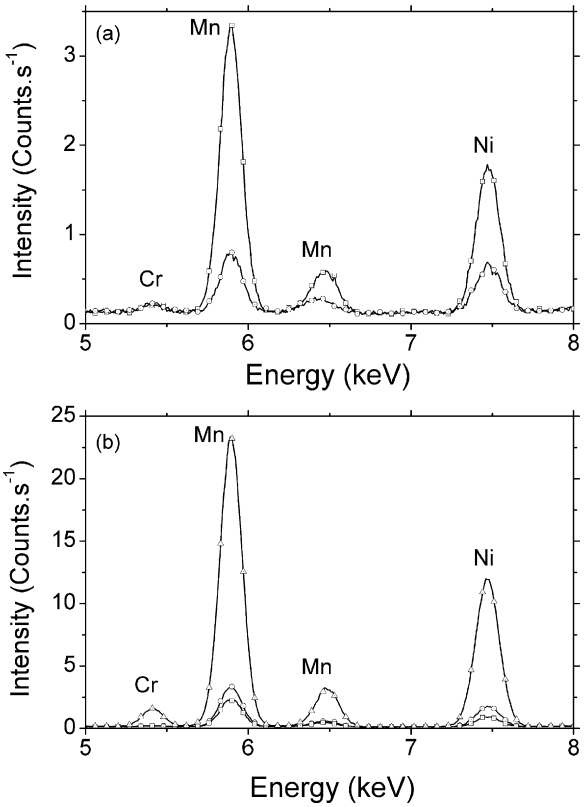

Fig. 14. TXRF spectra for (a) SAC700 with $Y = 0.05$ (circle) and $Y = 0.2$ (square) after soaking at 25 °C; (b) SAC700 (circle) and SAC900 (square) with $Y = 0.2$ after soaking at 25 °C and SAC900 $Y = 0.2$ (triangle) after soaking at 55 °C.

dissolution [10,15,16]. To study if the $LiCr_{2Y}Ni_{0.5-Y}Mn_{1.5-Y}O_4$ spinels were dissolved several samples was soaked in the electrolyte at 25 °C and at 55 °C for a week (see details in Section 2). The Cr, Ni and Mn concentration were determined by TXRF. As the SAC700 spinels showed the lowest capacity retentions (Fig. 12, Table 2) several of these samples were used to determine the influence of Cr-content on the dissolution process. In Fig. 14a, the TXRF spectra of the SAC700 samples with $Y = 0.05$ and 0.2 soaked at 25 °C are shown. In both spectra the Cr–K, Ni–K and Mn–K lines are observed. It indicates that for the two samples, the three cations were dissolved from the spinel. The TXRF peak intensities for the sample with $Y = 0.05$ are smaller (Fig. 14a) showing that dissolution is lower for this sample. For the SAC700 with $Y = 0.2$, the concentration of manganese, which is the most abundant cation in the spinel, was 5.0 ppm. Taking into account the sample mass used (80 mg) the Mn concentration for full dissolution of the spinels was ≈3100 ppm; thus, the percentage of manganese dissolved for this sample was 0.18%. For the sample with $Y = 0.05$, the Mn concentration was only 1.1 ppm; i.e., about five times lower than sample with $Y = 0.2$. The TXRF analysis shows that the cation dissolution increases with increasing the Cr-content, and it is one of the causes that could explain the diminution of QRt-40 observed for the SAC samples with $Y > 0.1$.

To study the effect of the cycling temperature, we have soaked several $LiCr_{0.4}Ni_{0.3}Mn_{1.3}O_4$ ($Y = 0.2$) samples at 25 °C and at 55 °C. The corresponding TXRF spectra are plotted in Fig. 14b. In both cases the K-lines of the three cations are observed showing that spinels dissolution also occurs at high temperature. In fact, the TXRF peak intensities of the SAC900 sample soaked at 55 °C are the highest indicating that spinel dissolution is larger at high temperature. For instance, Mn concentration in the electrolyte increases from ≈5 ppm for the samples soaked at 25 °C to 65.8 ppm for the SAC900 spinel at 55 °C; so, the Mn dissolution percentage rises from ≈0.15 to 2.1%, respectively. Nevertheless, the comparison of the cycling performances shows that QRt-40 for the SAC700 samples at 25 °C is always lower than those of the SAC900 spinels, even when these latter are cycled at 55 °C (Fig. 12). These results clearly indicate that, albeit the dissolution of the spinel is a significant factor, it is not the main cause to manage the cycling behavior of the $LiCr_{2Y}Ni_{0.5-Y}Mn_{1.5-Y}O_4$ spinels. Lack of correlation between dissolution data and cycling performances showing that the spinel dissolution it is not the sole factor responsible of capacity fade in $LiMn_2O_4$-based electrodes has been previously reported [21].

The oxidation of the electrolyte at the high potentials reached at the end of charge has been proposed as another factor responsible for the capacity loss of $LiMn_2O_4$-based cathodes [16,17]. Electrochemical impedance spectroscopy (EIS) is a useful tool to study the electrolyte degradation because this reaction gives way to formation of a corrupted solid electrolyte interface (SEI) with poorer Li^+ and electronic conductivities on the cathode surface [15–17]. This passivating film increases the cell impedance during cycling [51]. We have studied by EIS several SAC900 cells at 55 °C. As an example, in the inset of Fig. 15, the impedance plots for the $Y = 0.2$ sample before cycling and after the 40th cycle are compared. For the former cell the Nyquist plot shows an arc whose associated capacitance is 1.2E−5 F as deduced from the ideal equation $(RC/2\pi f) = 1$ where f is the frequency at the arc maximum, R is the arc resistance and C is the arc capacitance. It is ascribed to SEI formed on the cathode surface [16]. The arc is shifted from the origin giving rise to a pure resistance that is attributed to electrolyte resistance (R_{Elec}) [16]. For the cycled cell, the impedance plot also shows a pure resistance at the highest frequencies ascribed to the electrolyte and two arcs. The high-frequency arc has an associated capacitance of 3.1E−6 F which is similar to the arc found before cycling due to SEI. From comparison of the impedance plots of the cells before and after cycling we find: (i) an increase in the electrolyte resistance from 2 to 7 Ω after cycling, and (ii) a large increase in the arc resistance ascribed to SEI from 8 to 22 Ω. The increase of both resistances clearly shows that electrolyte degradation takes place during the cycling of the $Li//LiCr_{2Y}Ni_{0.5-Y}Mn_{1.5-Y}O_4$ cells. This collateral reaction explains why for every cycle the charge capacity is higher than the corresponding discharge one; that is, why the coulombic

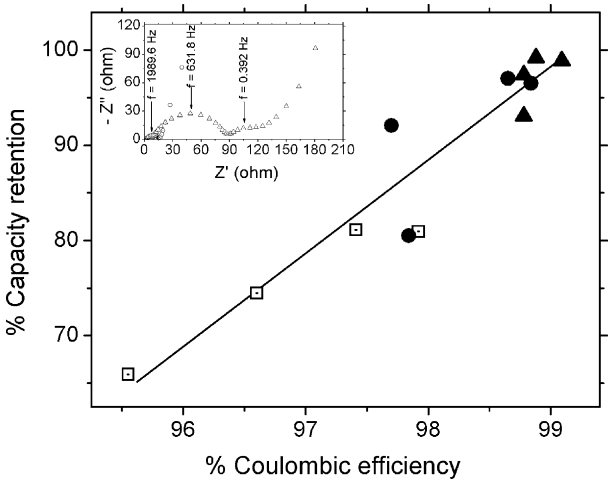

Fig. 15. Capacity retention after 40 cycles vs. coulombic efficiency for the SAC700 (square) and SAC900 (triangle) spinels cycled at 25 °C, and for the SAC900 spinels (circle) at 55 °C. The inset shows the Nyquist plots of the Li-cell with the SAC-900 $Y = 0.2$ cathode before cycling (circle), after the 40th cycle at 55 °C (triangle), and the corresponding Boukamp-fits.

Table 3
Synthesis method, particle size and electrochemical performances at 25 °C and at 55 °C for selected doped and undoped $LiNi_{0.5}Mn_{1.5}O_4$ spinels

Sample	Synthesis method	Thermal treatment	Particle size (μm)	Discharge capacity ($mAh\,g^{-1}$)	Cycle number	Capacity retention (%)	Reference
$LiNi_{0.5}Mn_{1.5}O_4$	Sol–gel	600 °C/24 h	–	110	32	95	[19]
$LiNi_{0.5}Mn_{1.5}O_4$	Emulsion drying	750 °C/24 h 850 °C/24 h	0.05 0.2	110 110	50 50	91 55	[36]
$LiNi_{0.5}Mn_{1.5}O_4$	Polymer-assisted	800 °C	0.07–0.08	117	50	84	[29]
$LiNi_{0.5}Mn_{1.5}O_4$	Spray-drying	800 °C/24 h	<1	125 122 (55 °C)	50 50	76 30 (55 °C)	[38]
$LiNi_{0.5}Mn_{1.5}O_4$	Sol–gel	850 °C/10 h	0.3–0.5	140 135 (55 °C)	50 50	92 27 (55 °C)	[12]
	Sol–gel + coated ZnO	850 °C/10 h	0.3–0.5	137 135 (55 °C)	50 50	94 98 (55 °C))	
$LiNi_{0.5}Mn_{1.5}O_4$	Sol–gel	750 °C	1.5	138 132 (50 °C)	50 50	98 34 (50 °C)	[45]
	Composite carbonate	700 °C/24 h	0.05–0.1	141 139 (50 °C)	50 50	97 96 (50 °C)	
$LiNi_{0.5}Mn_{1.5}O_4$	Hydroxide precursor	900 °C, O_2/12 h	–	131	50	92	[33]
$LiCr_{0.1}Ni_{0.45}Mn_{1.45}O_4$			–	134	50	98	
$LiCr_{0.2}Ni_{0.3}Mn_{1.5}O_4$			–	138	50	96	
$Li_{1.016}Cr_{0.05}Ni_{0.45}Mn_{1.484}O_4$			–	138	50	93	
$Li_{1.026}Ni_{0.42}Mn_{1.474}Fe_{0.08}O_4$	Hydroxide precursor	900 °C, O_2/12 h	–	131	50	95	[23]
$LiNi_{0.42}Mn_{1.5}Zn_{0.08}O_4$			–	125	50	98	
$LiNi_{0.42}Mn_{1.42}Co_{0.16}O_4$			–	113	50	97	
$LiCr_{0.2}Ni_{0.4}Mn_{1.4}O_4$	Solution reaction	850 °C	1–3	128	50	94	[32]
$LiNi_{0.5}Mn_{1.5}O_4$	Sol–gel	800 °C/24 h	–	137	50	91	[34]
$LiCr_{0.03}Ni_{0.47}Mn_{1.5}O_4$			–	137	50	97	
$LiFe_{0.1}Ti_{0.1}Ni_{0.45}Mn_{1.35}O_4$	Precipitation	850 °C/16 h	0.1–0.2	120	30	98	[35]
$LiCr_{0.2}Ni_{0.4}Mn_{1.4}O_4$	Combustion	900 °C/1 h	0.570	128 140 (55 °C)	40 40	99 97 (55 °C)	This work

Data for SAC900 $LiCr_{0.2}Ni_{0.4}Mn_{1.4}O_4$ synthesized in this work have been included.

efficiency (C_{Eff}) is <100% (Table 2). In Fig. 15 the capacity retention as a function of the coulombic efficiency is plotted. Data in this figure illustrate the strong correlation between the cycling performances of the SAC samples and their coulombic efficiency. In fact, an almost linear rise of QRt-40 on increasing C_{Eff} is observed. It indicates that the cycling performances are notably enhanced on decreasing the electrolyte degradation. The SAC900 samples with $Y \leq 0.1$ cycled at 25 °C have the highest C_{Eff} and they exhibit the largest capacity retentions (Table 2). In an opposite way, the coulombic efficiency of the SAC700 samples is lesser than that of SAC900 ones, even at 55 °C. Thus, the SAC700 with $Y = 0.2$ having the lowest C_{Eff} (95.55%) shows the worse cycling performances (QRt-40 = 65.93%). To explain all these results it is important to remind that the main difference between the SAC700 and SAC900 spinels is their particle size (Fig. 5, Table 1). As the particle size of the SAC900 samples is larger, they have a lower electrolyte/cathode interface to provoke undesirable oxidation reactions which explains their higher coulombic efficiency and superior cycling performances.

Finally, we have considered helpful to situate the electrochemical features of our samples among those reported in the literature for 5 V $LiNi_{0.5}Mn_{1.5}O_4$-based cathodes. In Table 3, data for the SAC900 $LiCr_{0.2}Ni_{0.4}Mn_{1.4}O_4$ are compared with those of selected doped and undoped $LiNi_{0.5}Mn_{1.5}O_4$ spinels. At room temperature, the cycling performances of our spinel (QRt-40 = 98.89%) is situated among the best reported in the literature. This value, which is higher than reported for undoped $LiNi_{0.5}Mn_{1.5}O_4$ samples, confirms the improvement of the cyclability of this spinel by doping at room temperature. Besides, the SAC900 $LiCr_{0.2}Ni_{0.4}Mn_{1.4}O_4$ maintain a high capacity retention at 55 °C, QRt-40 = 97.03%. This is up to the best of our knowledge, the only result existing in the literature on high-temperature cycling behavior of doped $LiNi_{0.5}Mn_{1.5}O_4$ cathodes. It permits us to demonstrate for the first time that metal doping is a useful way to improve the cycling performances of this 5 V $LiNi_{0.5}Mn_{1.5}O_4$-based cathodes a high temperature.

5. Conclusions

The sucrose-aided combustion method is a rapid, cheap and straightforward method to synthesize Cr-doped $LiNi_{0.5}Mn_{1.5}O_4$ spinels. Further thermal treatment of the "as-prepared" samples at 700 and 900 °C yields pure and single phase spinels as deduced from XRD and TG-DTA studies. X-ray data also show that: (i) Cr^{3+} randomly replaces the Ni^{2+} and the Mn^{3+} in 16d octahedral positions, and (ii) there are not any noticeable structural and compositional transformations on increasing the heating temperature. The study by TEM and SEM shows that: (i) all samples have submicrometric and homogeneous particle size, (ii) the particle size seems not to depend on the Cr-content, and (iii) the most remarkable difference between the SAC700 and the SAC900 spinels is the particle size, it rises from ≈50 to ≈500 nm on increasing the heating temperature from 700 to 900 °C. The analysis of the electrochemical properties permits to conclude that: (i) the discharge capacity (≈130 $mAh\,g^{-1}$) does not noticeably change with the synthesis conditions, and (ii) the cycling performances depend on the Cr-content but notably on the thermal treatment. The main factor that controls the cycling properties of the $LiCr_{2Y}Ni_{0.5-Y}Mn_{1.5-Y}O_4$ spinels is the electrolyte oxidation on charge. This reaction provokes the formation of a corrupted SEI which increases the cell impedance during cycling, as deduced by EIS. The electrolyte oxidation decreases on increasing the particle size. Thus, the SAC900 spinels, which have

the largest particle size, have the best cycling performances. Among the samples synthesized, the SAC900 spinels with $Y \leq 0.1$ exhibits the highest capacity retention, even at 55 °C (QRt-40 > 96%) being their cyclability >99.9% by cycle. The most highlighted point of this work is that it has been demonstrated for the first time that metal doping is a new approach to improve the cycling performances of 5 V $LiNi_{0.5}Mn_{1.5}O_5$-based electrodes at high temperature.

Acknowledgments

Financial support through the projects MAT2005-01606 (MEC), A/4957/06 (AECI) and the joint project CSIC-CNRST no. 2007MA0023 is thankfully recognized. M. Aklalouch thanks the AECI for the MAEC-AECI fellowship. R. Fernández-Ruiz is gratefully acknowledged for support on TXRF measurements.

References

[1] J.M. Tarascon, D. Guyomard, J. Electrochem. Soc. 138 (1991) 2864.
[2] M.M. Thackeray, Prog. Solid State Chem. 25 (1997) 1.
[3] M.S. Whittingham, Chem. Rev. 104 (2004) 4271.
[4] A.S. Arico, P. Bruce, B. Scrosati, J.M. Tarascon, W. Van Schalkwijk, Nat. Mater. 4 (2005) 366.
[5] B. Scrosati, S. Panero, P. Reale, D. Satolli, Y. Aihara, J. Power Sources 105 (2002) 161.
[6] T. Yoshida, K. Kitoh, T. Mori, H. Katsukawa, J.-I. Yamaki, Electrochem. Solid-State Lett. 9 (2006) A458.
[7] R.J. Gummow, A. de Kock, M.M. Thackeray, Solid State Ionics 69 (1994) 59.
[8] L. Pascual, M.L. Perez-Revenga, R.M. Rojas, J.M. Rojo, J.M. Amarilla, Electrochim. Acta 51 (2006) 3193.
[9] G.G. Amatucci, C.N. Schmutz, A. Blyr, A.C. Sigala, A.S. Gozdz, D. Larcher, J.M. Tarascon, J. Power Sources 69 (1997) 11.
[10] A. Du Pasquier, A. Blyr, P. Courjal, D. Larcher, G. Amatucci, B. Gérand, J.M. Tarascon, J. Electrochem. Soc. 146 (1999) 428.
[11] M.M. Thackeray, Y. Shao-Horn, A.J. Kahaian, K.D. Kepler, E. Skinner, J.T. Vaughey, S.A. Hackney, Electrochem. Solid-State Lett. 1 (1998) 7.
[12] Y.K. Sun, Y.S. Lee, M. Yoshio, K. Amine, Electrochem. Solid-State Lett. 5 (2002) A99.
[13] H.C. Wang, C.H. Lu, J. Power Sources 119 (2003) 738.
[14] M.A. Monge, J.M. Amarilla, E. Gutierrez-Puebla, J.A. Campa, I. Rasines, ChemPhysChem 4 (2002) 367.
[15] P. Arora, R.E. White, M. Doyle, J. Electrochem. Soc. 145 (1998) 3647.
[16] D. Aurbach, J. Power Sources 89 (2000) 206.
[17] C. Sigala, A. Le Gal La Salle, Y. Piffard, D. Guyomard, J. Electrochem. Soc. 148 (2001) A812.
[18] C. Sigala, D. Guyomard, A. Verbaere, Y. Piffard, M. Tournoux, Solid State Ionics 81 (1995) 167.
[19] Q. Zhong, A. Bonakdarpour, M. Zhang, Y. Gao, J.R. Dahn, J. Electrochem. Soc. 144 (1997) 205.
[20] S. Mandal, R.M. Rojas, J.M. Amarilla, P. Calle, N.V. Kosova, V.F. Anufrienko, J.M. Rojo, Chem. Mater. 14 (2002) 1598.
[21] Y. Shin, A. Manthiram, Chem. Mater. 15 (2003) 2954.
[22] H. Kawai, M. Nagata, H. Kageyama, H. Tukamoto, A.R. West, Electrochim. Acta 45 (1999) 315.
[23] T.A. Arunkumar, A. Manthiram, Electrochem. Solid-State Lett. 8 (2005) A403.
[24] J.M. Amarilla, R.M. Rojas, F. Pico, L. Pascual, K. Petrov, D. Kovacheva, M.G. Lazarraga, I. Lejona, J.M. Rojo, J. Power Sources 174 (2007) 1212.
[25] D. Djian, F. Alloin, S. Martinet, H. Lignier, J.Y. Sanchez, J. Power Sources 172 (2007) 416.
[26] I. Belharouak, Y.K. Sun, W. Lu, K. Amine, J. Electrochem. Soc. 154 (2007) A1083.
[27] J.H. Kim, S.T. Myung, C.S. Yoon, S.G. Kang, Y.-K. Sun, Chem. Mater. 16 (2004) 906.
[28] N. Amdouni, K. Zaghib, F. Gendron, A. Mauger, C.M. Julien, Ionics 12 (2006) 117.
[29] J.C. Arrebola, A. Caballero, M. Cruz, L. Hernán, J. Morales, E. Rodríguez Castellón, Adv. Funct. Mater. 16 (2006) 1904.
[30] Y. Talyosef, B. Markovsky, R. Lavi, G. Salitra, D. Aurbach, D. Kovacheva, M. Gorova, E. Zhecheva, R. Stoyanova, J. Electrochem. Soc. 154 (2007) A682.
[31] Y. Terada, K. Yasaka, F. Nishikawa, T. Konishi, M. Yoshio, I. Nakai, J. Solid State Chem. 156 (2001) 286.
[32] Y. Sun, Z. Wang, X. Huang, L. Chen, J. Power Sources 132 (2004) 161.
[33] T.A. Arunkumar, A. Manthiram, Electrochim. Acta 50 (2005) 5568.
[34] S.B. Park, W.S. Eom, W.I. Cho, H. Jang, J. Power Sources 159 (2006) 679.
[35] B. León, J.M. Lloris, C. Perez-Vicente, J.L. Tirado, Electrochem. Solid-State Lett. 9 (2006) A96.
[36] S.T. Myung, S. Komaba, N. Kumagai, H. Yashiro, H.T. Chung, T.H. Cho, Electrochim. Acta 47 (2002) 2543.
[37] M. Kunduraci, G.G. Amatucci, J. Electrochem. Soc. 153 (2006) A1345.
[38] H.M. Wu, J.P. Tu, Y.F. Yuan, Y. Li, X.B. Zhao, G.S. Cao, Electrochim. Acta 50 (2005) 4104.
[39] Y. Fan, J. Wang, Z. Tang, W. He, J. Zhang, Electrochim. Acta 52 (2007) 3870.
[40] J. Laugier, A. Filhol, CelRef, PC version (unpublished), ILL, Grenoble, France, 1991.
[41] S. Mandal, J.M. Amarilla, J. Ibáñez, J.M. Rojo, J. Electrochem. Soc. 148 (2001) A24.
[42] R.M. Rojas, J.M. Amarilla, L. Pascual, J.M. Rojo, D. Kovacheva, K. Petrov, J. Power Sources 160 (2006) 529.
[43] A. Caballero, M. Cruz, L. Hernán, J. Morales, E. Rodríguez-Castellón, J. Electrochem. Soc. 152 (2005) A552.
[44] R.M. Rojas, K. Petrov, G. Avdeev, J.M. Amarilla, L. Pascual, J.M. Rojo, J. Therm. Anal. Calorim. 90 (2007) 67.
[45] Y.S. Lee, Y.K. Sun, S. Ota, T. Miyashita, M. Yoshio, Electrochem. Commun. 4 (2002) 989.
[46] R.D. Shannon, C.T. Prewitt, Acta Crystallogr., Sect. B: Struct. Crystallogr. Cryst. Chem. 25 (1969) 925.
[47] P. Strobel, F. Le Cras, L. Seguin, M. Anne, J.M. Tarascon, J. Solid State Chem. 135 (1998) 132.
[48] C. Sigala, A. Le Gal La Salle, Y. Piffard, D. Guyomard, J. Electrochem. Soc. 148 (2001) A819.
[49] L. Pascual, H. Gadjov, D. Kovacheva, K. Petrov, P. Herrero, J.M. Amarilla, R.M. Rojas, J.M. Rojo, J. Electrochem. Soc. 152 (2005) A301.
[50] C. Sigala, A. Verbaere, J.L. Mansot, D. Guyomard, Y. Piffard, M. Tournoux, J. Solid State Chem. 132 (1997) 372.
[51] R. Alcantara, M. Jaraba, P. Lavela, J.L. Tirado, J. Electroanal. Chem. 566 (2004) 187.